DEPARTMENT OF MECHANICAL ENGINEERING AND MECHANICS
SCHOOL OF ENGINEERING
OLD DOMINION UNIVERSITY
NORFOLK, VIRGINIA

RESULTS OF BORON-ALUMINUM THRUST STRUCTURE TEST

By

M. W. Hyer

and

Michael C. Lightfoot

Interim Report

Prepared for the
National Aeronautics and Space Administration
Langley Research Center
Hampton, Virginia

Under
Research Grant NSG 1167
John G. Davis, Jr., Technical Monitor
Materials Division

December 1976

OLD DOMINION UNIVERSITY RESEARCH FOUNDATION

DEPARTMENT OF MECHANICAL ENGINEERING AND MECHANICS
SCHOOL OF ENGINEERING
OLD DOMINION UNIVERSITY
NORFOLK, VIRGINIA

RESULTS OF BORON-ALUMINUM THRUST STRUCTURE TEST

By

M. W. Hyer

and

Michael C. Lightfoot

Interim Report

Prepared for the
National Aeronautics and Space Administration
Langley Research Center
Hampton, Virginia

Under
Research Grant NSG 1167
John G. Davis, Jr., Technical Monitor
Materials Division

Submitted by the
Old Dominion University Research Foundation
Norfolk, Virginia 23508

December 1976

ABSTRACT

This report presents the results of testing-to-failure a two member boron-aluminum thrust structure. The structure represented one section of a more complex planar truss and was designed to test the integrity of a diffusion bonded joint. The structure failed at 107 percent of the ultimate design load in the diffusion bond region. Strain gages and displacement transducers were used to measure loads and deflections of the truss. The experimentally derived axial loads, bending moments and torsion in the various members are presented and compared with predicted values. In general, the comparison is quite good.

TABLE OF CONTENTS

LIST OF TABLES

LIST OF FIGURES

LIST OF FIGURES (Concluded)

RESULTS OF BORON-ALUMINUM THRUST STRUCTURE TEST

By

M. W. Hyer[1] and Michael C. Lightfoot[2]

INTRODUCTION

Future space travel will require lighter, more efficient space transportation systems. Lighter spacecraft will result in higher payloads and less energy consumption for travel and maneuver. The use of advanced fiber-reinforced composites as a structural material is one way to achieve a weight reduction. Advanced composites increase structural efficiency and thereby offer a weight savings over conventional structural materials such as titanium or aluminum. Ultimately an entire space vehicle might be constructed of composite materials, but at present, studies are centered on selective use of composites to reinforce primary structural members or to lighten certain weight-critical areas. Whenever composites and conventional materials are used together, close attention must be given to fastening these materials together. Standard techniques such as welding, riveting, and bolting do not lend themselves to composites because these techniques, when applied, allow discontinuity of fibers and abrupt changes in material properties. These methods must be avoided to achieve maximum structural efficiency when using fiber or reinforced composite materials.

This work presents experimental results of testing-to-failure a 1/3 scale boron-aluminum reinforced titanium thrust structure. The structure was tested at the Langley Research Center and was fabricated by General Dynamics to test the integrity of a diffusion-bonded step-lapped joint in a compression member. The joint was designed to transfer the load from the boron-aluminum to the titanium. The structure was the second of its type tested, being

[1] Assistant Professor, Department of Mechanical Engineering and Mechanics, Old Dominion University, Norfolk, Virginia 23508.

[2] Research Assistant, Department of Mechanical Engineering and Mechanics, Old Dominion University, Norfolk, Virginia 23508.

preceded by a boron-epoxy reinforced titanium structure (ref. 1), and was predicted to fail in the diffusion-bond region. In the previous truss, consisting of a boron-epoxy reinforced compression member and a boron-epoxy reinforced tension member, the tension member failed at 118 percent of the ultimate design load. Thus the ultimate strength of the compression member was not determined. For this reason, a modification of the design was incorporated in the boron-aluminum truss.

DESCRIPTION OF STRUCTURE

Figure 1 shows a planar idealization of the booster thrust structure. An unsymmetric loading, representative of gimbaled engines, presents the most critical case of loading and is the case studied in this report. Figure 2 shows internal load distribution in the test segment.

The truss consisted of four major components: the compression tube, the tension member, the joint cluster, and the loading ram.

Of particular interest was the compression member, shown in figure 3. The member consisted of two titanium collars and a boron-aluminum tube. Each collar was 228.6 mm long with a constant outer diameter and an inner diameter that varied along the length. The fabrication of the boron-aluminum section consisted of rolling a monolayer unidirectional tape to a wall thickness of 15 plies. The precut tape had tapered ends such that when rolled it produced discrete helical steps at both ends of the tube section. After placing the collars over these stepped regions, the titanium and boron-aluminum were diffusion bonded together. The diffusion bond spanned a region of 127 mm.

Since one of the primary concerns was the ultimate strength of the compression member, a complementary boron-aluminum tension member was not fabricated. Instead, a dummy member was fabricated of an alloy steel. This member was designed to have approximately the same extensional stiffness as the previous boron-epoxy tension member. The details of the member are shown in figures 4 and 5.

The joint cluster, a hollowed out titanium member, was designed specifically for the truss fixture. This joint is a two-dimensional extraction of a typical

three-dimensional clustered connector. The loading ram was not meant to represent actual engine attachments but was designed as a means of transferring load.

TEST PROCEDURE

Figure 6 shows the section mounted in the test position. The load was applied by a hydraulic jack. The load was actually applied through a round pin, which in turn rested on a flat plate and rollers. This mechanism allowed only vertical loads to be applied to the ram.

To determine the truss reactions to the applied load, strain gages and direct current displacement transformers (DCDT's) were used to record strains and deflections. Single and rosette gages were mounted along the length of the compression tube with all single gages aligned axially on the top and bottom of the tube and the 0° arm of the 0°-45°-90° rosettes aligned axially along the sides of the tube. Figures 7 and 8 show gage locations on the tube. With this arrangement axial force, vertical and side bending, torsional moment and vertical shear load could be determined. In addition, four axial gages were put on the tension member to check the axial load and vertical and side bending in that member. DCDT's were located to monitor what primarily would be rigid body motion of the joint cluster. Figure 9 shows the locations of the DCDT's.

Alignment of the test section was checked by applying small loads and monitoring strains and displacements. A survey of the data at a low load level indicated a tendency of the truss to deflect laterally. At that time it was not known whether the deflection was due to misalignment of the loading or due to eccentricities in the truss. To monitor the loading, four axial strain gages were placed on the loading ram to measure axial load and fore-and-aft and side-to-side bending. A second low load test indicated side bending of the ram. Shimming at various locations and alignment of the hydraulic loading jack helped eliminate some of the bending. Vertical alignment of the entire test assembly on the backstop was checked with a surveyor's transit. It was found that although the upper and lower backstop mounts were vertically aligned, the top of the joint cluster was 2.54 mm further to the right, when viewed from the front, than the bottom of the ram. This was basically an assembly eccentricity. In an effort to align the ram vertically, bolts at various joints were

loosened in hopes of finding enough tolerance in the bolt holes to straighten the ram and joint cluster. The necessary tolerance did not exist and so the bolts were tightened to a torque of 54 Nm. Since the misalignment had not been eliminated, support rods approximately 1 m long and 15.88 cm in diameter were attached to the cluster and run horizontally to the backstop to restrain any tendency of the truss to deflect sideways. To determine how much load was transmitted to the support rods, axial strain gages were placed on the top and bottom of the right rod.

Table 1 lists all strain gages and DCDT's and their respective locations.

TEST RESULTS

After the alignment procedures, the truss was loaded to failure. Load, strain, and displacement were recorded every five seconds from 0 to 710 kN. From 710 to 747 kN they were recorded every two seconds. Within a load range of 747 to 770 kN data was recorded at one-second intervals. Finally after 770 kN the data was recorded at two-second intervals until failure. The truss failed with a force of 834 kN on the loading ram. This load was 107 percent of the design ultimate load. The failure occurred in the upper diffusion bonded region of the compression tube when the inner boron-aluminum tube telescoped inside of the titanium end fitting. Figure 10 shows the failed compression tube, and figure 11 shows a detail of the titanium end fitting. Although the load carrying capacity of the truss reached 834 kN, the strain gage data indicated there was a localized failure on the top side of the upper bond at a load of 456 kN (58.6 percent design ultimate). Figure 12 shows strain at strain gage location 11 and indicates a sudden decrease in strain at that load level. Gages 10, 12, 20A, 33, and 43A also show a sudden decrease in strain level but not the same magnitude as at gage 11. Although the ram force did not change, strain recordings indicated a sudden release of load in the region of the gage. Except for a slight increase in strain level at 20B, 42B, and 43B, there doesn't appear to be a clear indication of the load increasing elsewhere. DCDT data indicated that the top of the joint cluster jumped forward and slightly to the right at the time of this local failure. As the load continued to increase, there were other sudden decreases in strain

indicating the failure was spreading. Figure 13 shows load versus strain at locations 43C, 43B, 43A, 42B, and 33, and from these plots these other sudden changes are evident. Except for a few slight jumps at these same load levels in several other gages, the majority of the gages showed linear load-strain behavior up to failure.

Figures 14 through 19 show, respectively, the axial compressive force, vertical bending moment, side bending moment, vertical shear and torsional moment along the compression tube as a function of applied load. Each figure has the experimentally derived loads for 50 percent and 100 percent design ultimate load and, in some cases, the theoretical load based on elementary statics. Computations were done for 25, 50, 58.6, 75, 100, and 107 percent ultimate load. The 58.6 percent load level was chosen to determine if there was an adverse loading condition when the local failure occurred, and the 107 percent level was chosen since that is the failure load. The 25, 50, 75, and 100 percent load levels were chosen as convenient intervals. Since there were no unusual conditions at any load level, 50 percent and 100 percent were chosen as representative.

The axial force in the compression member was determined two ways: using top and bottom axial gage pairs and using side-to-side axial gage pairs. The vertical bending moment and side bending moment were computed using top and bottom and side-to-side axial gage pairs respectively. The vertical shear and torsional moments were computed using side-to-side rosettes. The sign conventions for these loads are indicated on the figures. The axial force, vertical bending moment and vertical shear are the primary loads on the tube and are of principal concern while the side-to-side bending and torsional moment, both of which should be zero, were computed to determine departure from the ideal loading situation. The value of Young's Modulus, E, used in computing the axial load and bending moment in the boron-aluminum section was determined by testing a short cutout segment of the failed compression tube. Appendix A gives the detailed results of this testing. The value of E used in the diffusion bonded region was determined from the rule of mixtures, and the value for each particular location is given in that appendix.

Tables 2, 3, and 4 respectively indicate the loads in the tension member, the loading ram, and the right support rod. The sign conventions for these

loads are shown on the figures. The values of E used in these calculations were taken from handbooks quoting commonly used values for the steel alloys in the components. Figure 20 shows the displacement of the ram and joint cluster. The displacement figures were drawn using the DCDT data and assuming rigid body behavior.

The experimental values of the axial force in the compression member compare well with the theoretical predictions in the boron-aluminum section. In the diffusion-bonded region, the comparison is not as good. In this region (figure 3) the material properties are changing with radial distance through the tube due to a transition from boron-aluminum to titanium. The rule of mixtures yields a "smeared out" or equivalent E value for a cross-section in this region of the tube. Since the elastic properties vary with radius, the strain varies with radius. Unless the strain gradient is small, there is no a priori reason to believe that multiplying surface strains by an equivalent E will yield the correct average stress. A better approximation to the average stress might be obtained if the rule-of-mixtures E was multiplied by a strain averaged using strains of the inner and outer radius. However, in this case as in others, only the outer radius strains could be conveniently measured. In addition, as previously mentioned, the boron-aluminum in this region tapers off in helical steps, producing stepped elastic properties. This transitional effect could well produce erratic readings, particularly if a gage is over a step.

Referring to figure 2, for design purposes, the compression member was considered to act as a beam column with a moment, shear force and axial load on the upper end and a shear force and axial load on the lower end. Because the elastic and geometric properties change along the length of the member, an analysis of the member is difficult. In addition, any deflection and rotation of the titanium cluster in the plane of the truss would generate an additional moment at the lower end of the compression tube. Thus, the loading on the member is quite complex and is coupled to the other members and no attempt was made to predict the shear and bending moments along the member. Figure 16 shows the experimentally derived moment distribution along the length of the compression member. If the member is not considered as a beam column, the bending moment distribution is linear with distance along the tube, starting at zero at

the lower end and reaching a maximum at the upper end. At the lower load levels, 25 percent and 50 percent, a somewhat linear distribution was evident. However, as the load increased, beam-column effects and rotation of the cluster became apparent. In addition, manufacturing eccentricities, basically an unknown, add other moments. General Dynamics made allowances for a .762 mm manufacturing eccentricity in their moment calculations. They assumed, for design purposes, that the moment due to the eccentricity added to the moments due to vertical loads. Because of the change in sign of the moment along the tube at the lower load levels, there probably was an eccentricity.

Figure 17 indicates that the side bending moment was substantial. At the 100 percent design load level, the side moment was one-third of the vertical moment. Although this condition wasn't desirable, it is felt there were no serious effects due to it.

Although vertical shear forces are generated in the compression tube, the magnitudes of the force and the accompanying deformations are not significant in governing the behavior of the truss. Figure 18 shows that the experimentally derived results are somewhat erratic. The shear force changes in magnitude and sign with the most erratic behavior being in the diffusion bond area.

In figure 19 the torsional loads also appear erratic in sign. Torsional loads can only be transferred to the tube through the ends, and thus the sign of the torsion should be constant along the length. The calculations show the torsional load changes sign with distance along the tube, a condition which cannot exist. At the lower load levels, the sign of the torsional load is constant along the boron-aluminum segment of the tube while in the diffusion area the sign and magnitude are constantly changing. The values of shear modulus in this area were determined using the rule of mixtures. Again, the erratic experimental results can partly be attributed to using surface strains as a measure of the stress throughout the cross section. At the high load levels it is not clear why the torsion changes sign in the middle of the tube. It might be noted that the magnitude of the torsional moment is so small that the strain gage errors (misalignment, electrical, etc.) might significantly affect the results.

Tables 2 and 3 indicate that the axial loads in the tension member and the ram are quite close to predictions. The bending moments in the tension member are insignificant. The fore and aft bending moment in the ram can be expected

due to the rotation of the ram-cluster assembly. The magnitudes of the moments are consistent with the magnitude of the outward displacement of the bottom of the ram. Ideally the side-to-side bending moment should be zero. However, as indicated earlier, eccentricities existed, and the nonzero moment results. The magnitude of the moment is consistent with these misalignments experience earlier.

Referring to table 4, as a result of the misalignment and eccentricities, the right support rod was subject to substantial axial load. The rotation of the joint cluster indicates that the rod should have bowed down. The strain gages indicate the rod bowed up. The Euler load for the rod, assuming simple supports, was 6.2 kN. The rod was not checked for initial straightness, but after failure of the truss, curvature was evident. The curvature was noted only after disassembly of the truss and unfortunately the orientation of the curvature, relative to the truss, was not recorded. Considering the strain gage data from the rod and the rotation of the joint cluster, one can only speculate that the axial compressive force in the rod coupled with an initial curvature to bow the rod up, overcoming any bow-down tendency due to cluster rotation.

Since the support rods were not of prime concern it is sufficient to say that they more than likely prevented side deflection and, consequently, out-of-plane buckling, which permitted a reliable evaluation of the truss members.

CONCLUSIONS

From the experimental results it is clear that the behavior of the truss was generally predictable. Failure occurred at 107 percent of the design ultimate. Predictions of the mode and level of failure were quite accurate and not sensitive to loading and assembly eccentricities. There was evidence of a localized failure at 58.6 percent of the design ultimate load, and, for this test, there did not appear to be any serious consequences. Whether this localized failure at the relatively low load level is characteristic of a diffusion-bonded joint can only be determined through careful experimentation or, if available, reexamination of similar test data. Had this occurred at 80 or 90 percent of ultimate it would not be as significant, but it is felt that this phenomena should be investigated further.

Table 1. Summary of strain gage and DCDT location.

Strain Gage No.	Location[1] (Comp. Tube) m	Strain Gage No.	Location[1] (Comp. Tube) m	Strain Gage No.	Location[1] (Comp. Tube) m
1	.1334	15A	.1778	21C	.8709
2	.1651	15B	.1778	22A	.9471
3	.1968	15C	.1778	22B	.9471
4	.2445	16A	.2445	22C	.9471
5	.3504	16B	.2445	23	.1334
6A[2]	.5244	16C	.2445	24	.1651
6B[2]	.5244	17A	.3504	25	.1968
6C[2]	.5244	17B	.3504	26	.2445
7	.5244	17C	.3504	27	.3504
8A	.5244	18A	.5244	28A	.5244
8B	.5244	18B	.5244	28B	.5244
8C	.5244	18C	.5244	28C	.5244
9	.6984	19A	.6984	29	.5244
10	.8043	19B	.6984	30A[2]	.5244
11	.8519	19C	.6984	30B[2]	.5244
12	.8837	20A	.8043	30C[2]	.5244
13	.9154	20B	.8043	31	.6984
14A	.1016	20C	.8043	32	.8043
14B	.1016	21A	.8709	33	.8519
14C	.1016	21B	.8709	34	.8837

(cont'd)

[1] Measured from lower end of compression tube.

[2] Not used in the ultimate test.

Table 1. Summary of strain gage and DCDT location (concl'd).

Strain Gage No.	Location[1] (Comp. Tube) m	Strain Gage No.	Location[1] (Comp. Tube) m
35	.9154	42A	.8043
36A	.1016	42B	.8043
36B	.1016	42C	.8043
36C	.1016	43A	.8709
37A	.1778	43B	.8709
37B	.1778	43C	.8709
37C	.1778	44A	.9471
38A	.2445	44B	.9471
38B	.2445	44C	.9471
38C	.2445	45	Mid-span Tension Member - Bottom
39A	.3504	46	Mid-span Tension Member - Left
39B	.3504	47	Mid-span Tension Member - Top
39C	.3504	48	Mid-span Tension Member - Right
40A	.5244	53	Support Rod Top
40B	.5244	54	Support Rod Bottom
40C	.5244	49	Loading Ram Right
41A	.6984	50	Loading Ram Back
41B	.6984	51	Loading Ram Left
41C	.6984	52	Loading Ram Front

[1] Measured from lower end of compression tube.

Table 2. Loads in tension member.

Percent Ultimate Load	Bending Moment Fore/Aft (Newton-meters)		Bending Moment Side/Side (Newton-meters)		Axial Force Fore/Aft (kilo-Newtons)		Axial Force Side/Side (kilo-Newtons)		Average Axial Force (kilo-Newtons)	
	Exp.	Theor.	Exp.	Theor.	Exp.[1]	Theor.	Exp.[1]	Theor.	Exp.[1]	Theor.
25	16.3	0	15.4	0	132.1	133.4	131.4	133.4	131.8	133.4
50	30.1	0	22.4	0	267.0	266.9	266.1	266.9	266.5	266.9
58.6	33.0	0	23.7	0	312.6	312.8	311.8	312.8	312.2	312.8
75	38.8	0	27.2	0	403.1	400.3	402.5	400.3	402.8	400.3
100	39.8	0	26.0	0	557.8	533.8	557.8	533.8	557.8	533.8
107	34.0	0	23.4	0	620.5	571.9	620.5	571.9	620.5	571.9

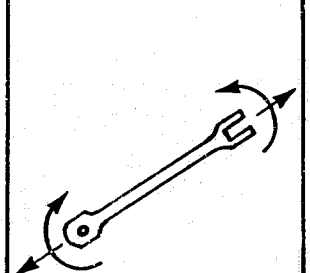

LEFT SIDE VIEW

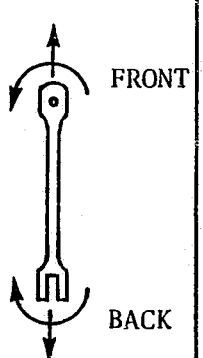

TOP VIEW

[1] These are values obtained from strain data and were derived from the data taken at the time the vertical load, as measured by the load cell in the hydraulic jack, was 25 percent, 50 percent, . . . etc. of 778.4 kN (see figure 2).

Table 3. Loads in loading ram.

Percent Ultimate Load	Bending Moment Fore/Aft (Newton-meters)		Bending Moment Side/Side (Newton-meters)		Axial Force Fore/Aft (kilo-Newtons)		Axial Force Side/Side (kilo-Newtons)		Average Axial Force (kilo-Newtons)	
	Exp.	Theor.	Exp.	Theor.	Exp.[1]	Theor.	Exp.[1]	Theor.	Exp.[1]	Theor.
25	754	0	237	0	206.2	194.6	189.1	194.6	197.7	194.6
50	1417	0	454	0	416.6	389.2	379.2	389.2	397.9	384.2
58.6	1578	0	707	0	489.3	456.1	447.9	456.1	468.6	456.1
75	1455	0	776	0	614.3	583.8	564.4	583.8	589.4	583.8
100	1062	0	1113	0	831.3	778.4	749.4	778.4	790.4	778.4
107	756	0	1006	0	884.7	834.0	794.0	834.0	839.3	834.0

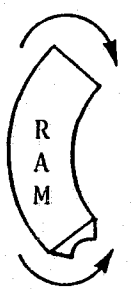

LEFT SIDE VIEW

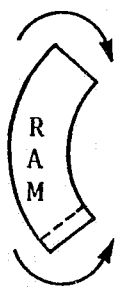

FRONT VIEW

[1] These are values obtained from strain data and were derived from the data taken at the time the vertical load, as measured by the load cell in the hydraulic jack, was 25 percent, 50 percent, . . . etc. of 778.4 kN (see figure 2).

Table 4. Loads in support rod.

Percent Ultimate Load	Bending Moment, M (Newton-meters)	Axial Force, P (Newtons)
25	5.2	1334.4
50	9.1	2636.3
58.6	9.8	3124.3
75	10.7	3970.7
100	11.0	4848.3
107	11.3	5173.0

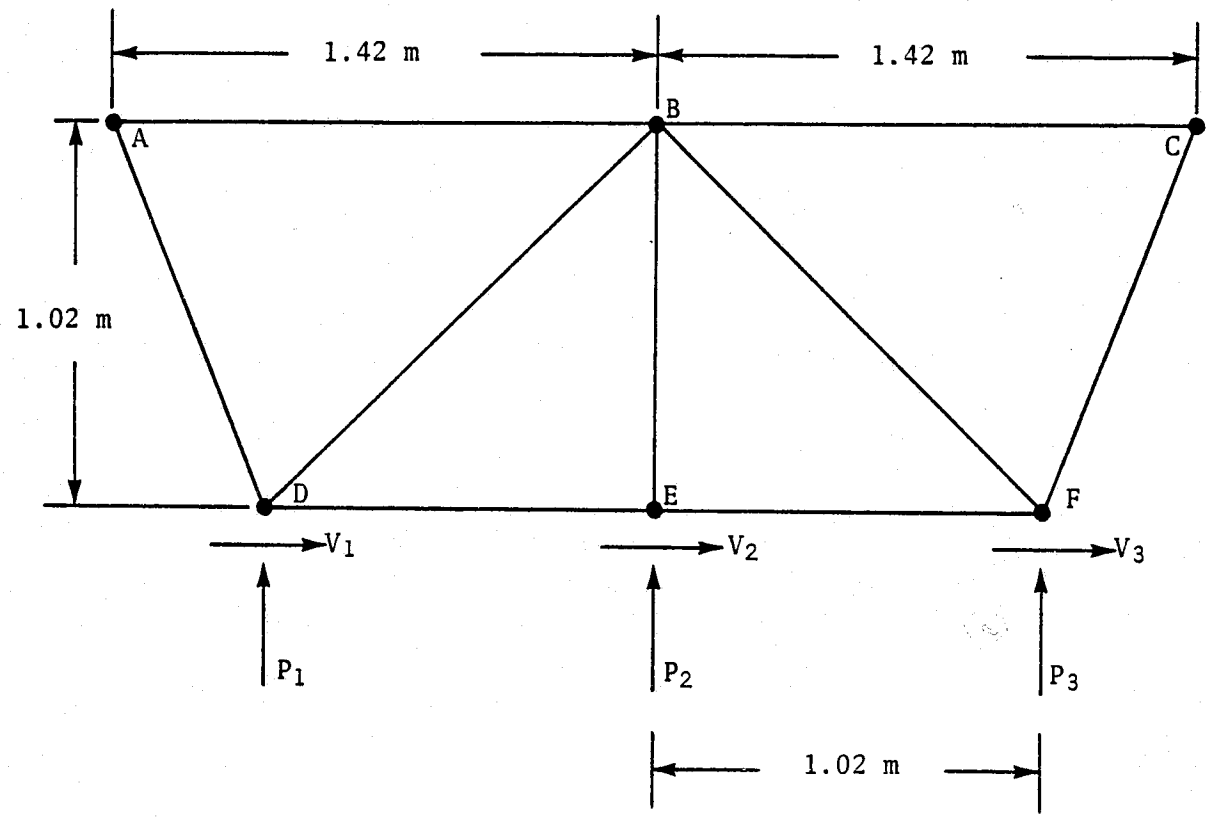

	Ultimate Applied Loads and Member Loads (kN)	
	Engines Symmetric	Engines Gimbaled
P_1	351.4	349.2
P_2	482.2	478.2
P_3	351.4	349.2
V_1	0	42.7
V_2	0	58.7
V_3	0	42.7
AB, BC	285.6	537.3
AD, CF	-636.1	-789.1
BD, BF	340.7	505.3
DE, EF	-477.7	-533.8
BE	-482.2	-478.2

Figure 1. Planar truss with idealized ultimate loads (ref. 1).

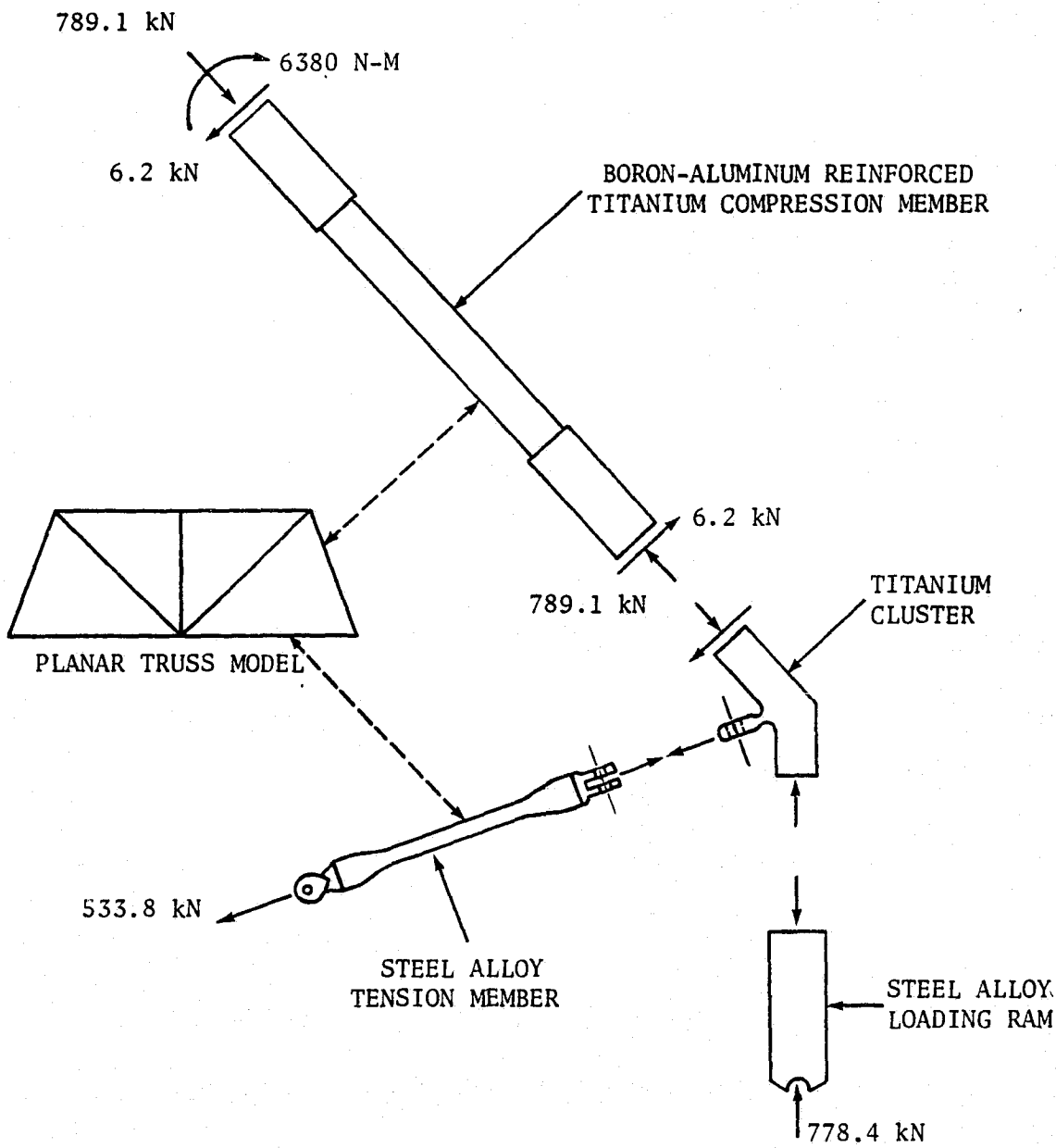

Figure 2. Internal loads distribution in test section.

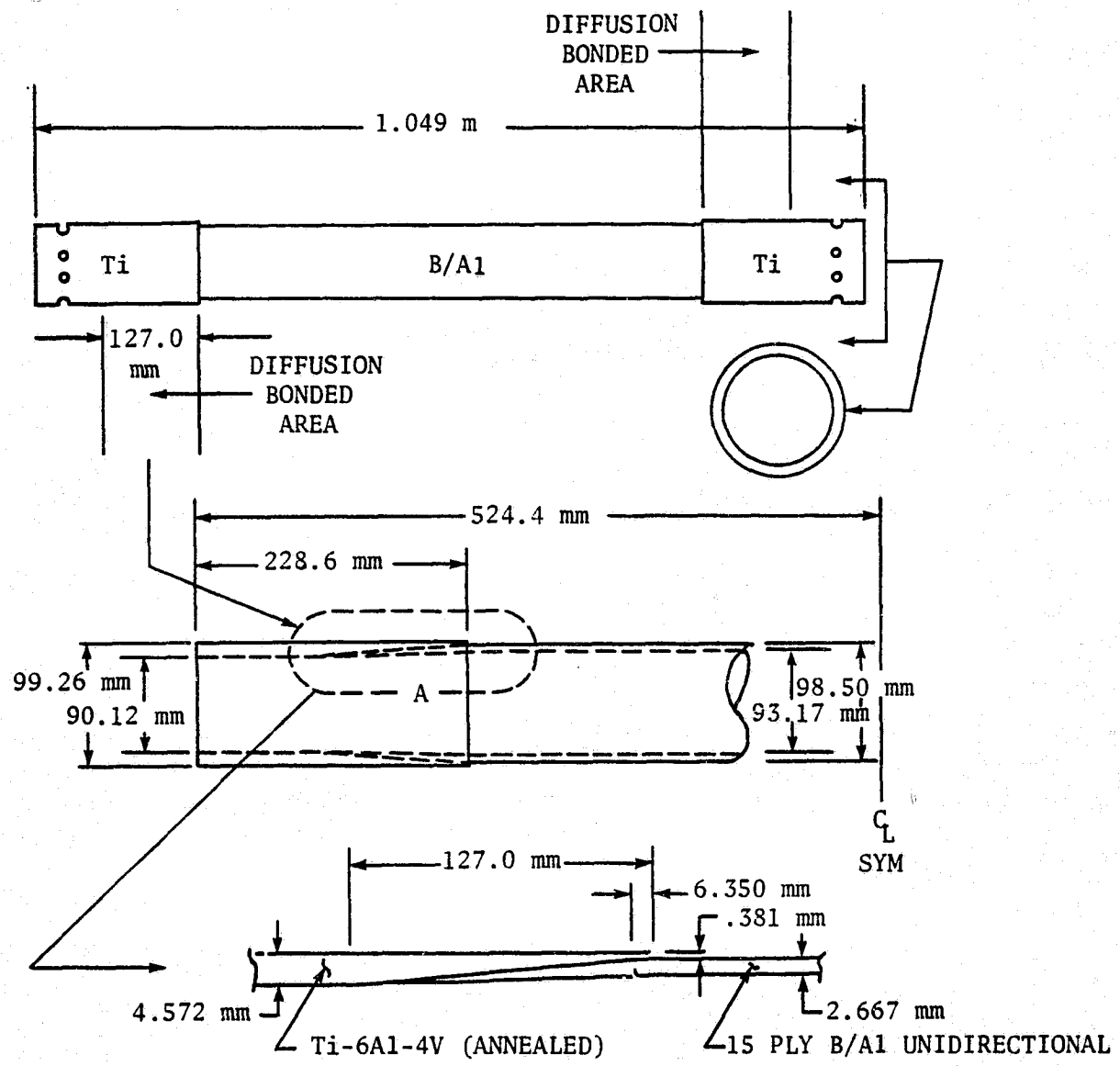

Figure 3. Details of boron-aluminum compression strut.

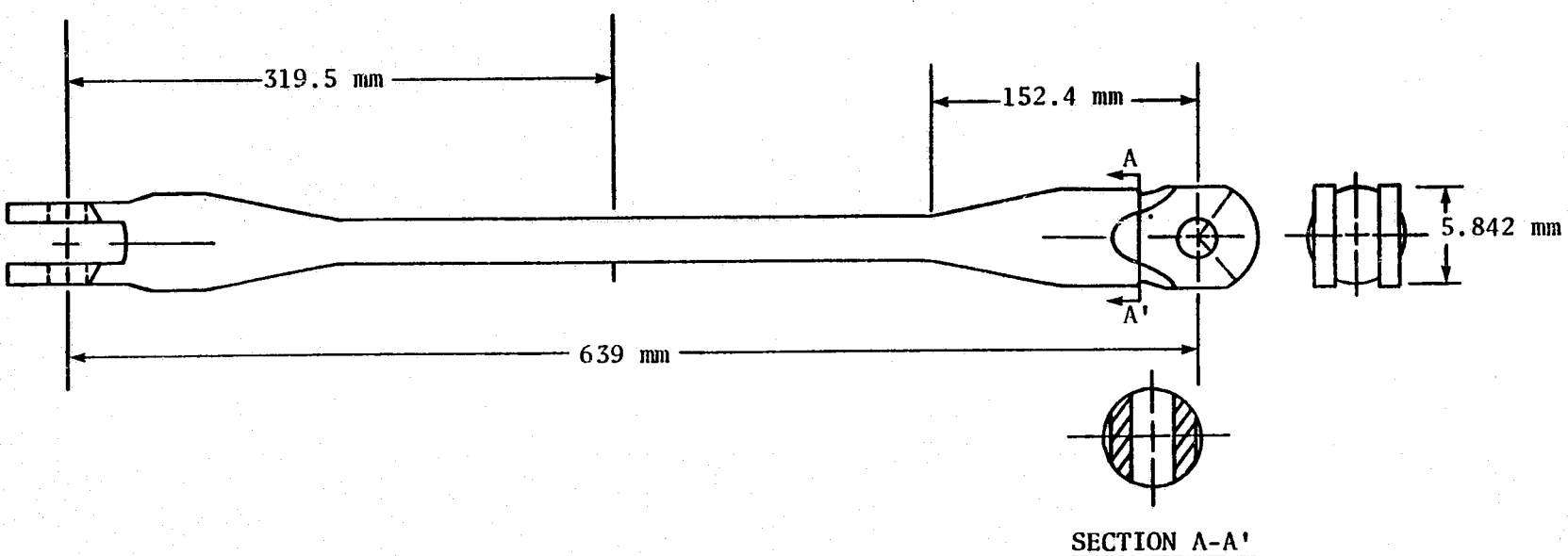

MATERIAL: Fe-17Cr-4Ni-4Cu

Figure 4. Geometry of the tension member.

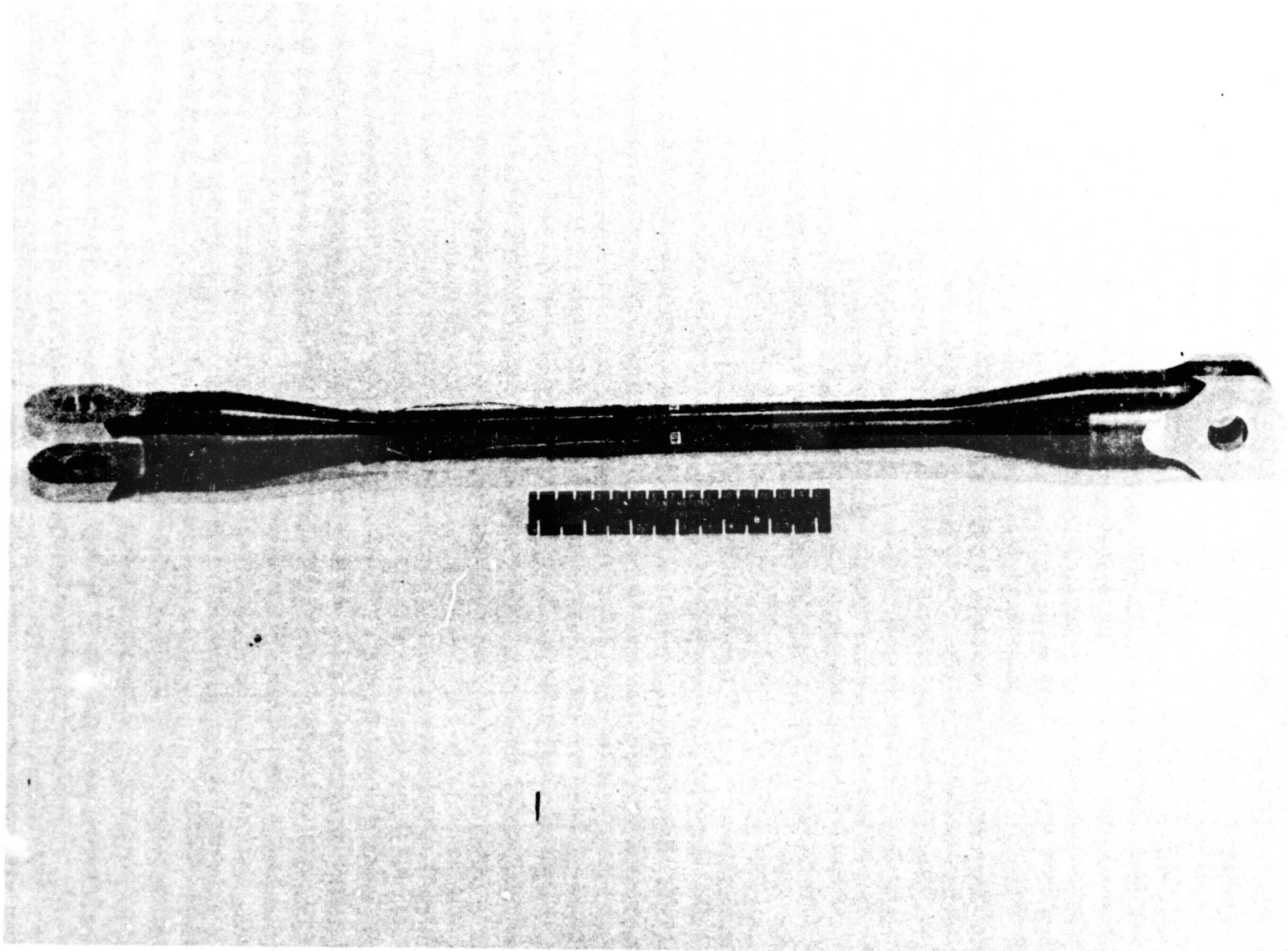

Figure 5. Tension member.

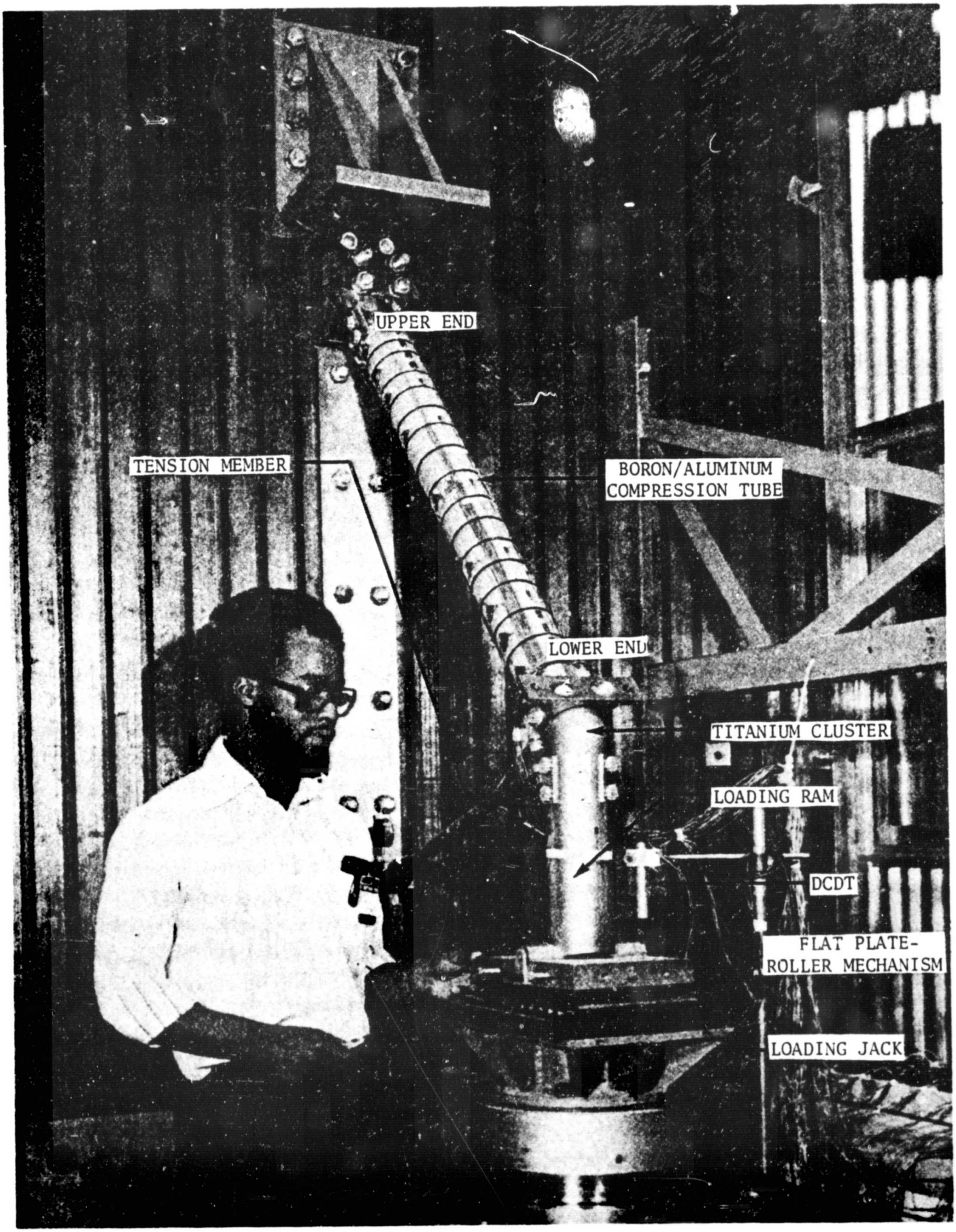

Figure 6. Test apparatus for truss structure.

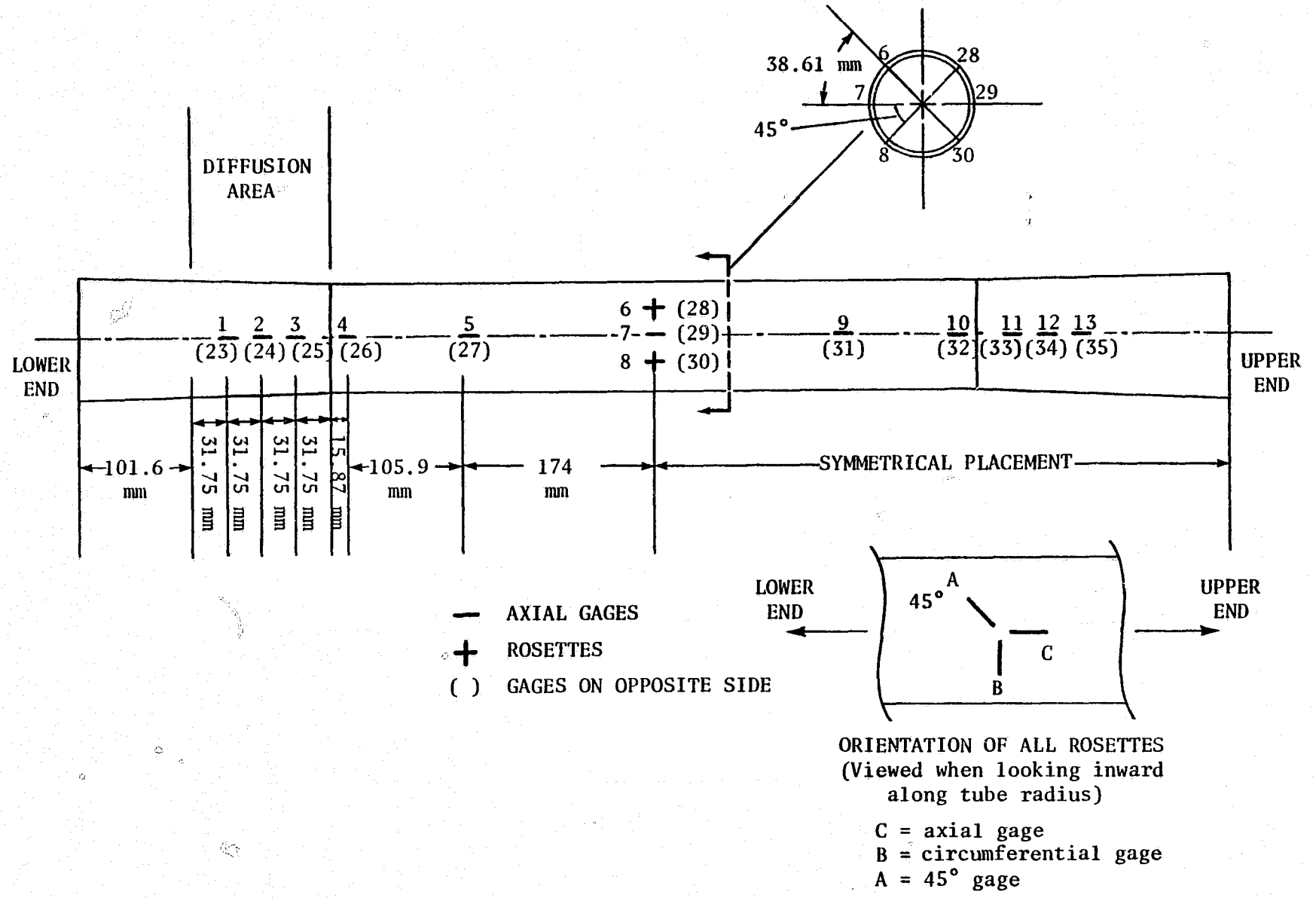

Figure 7. Top and bottom strain gage locations, top view.

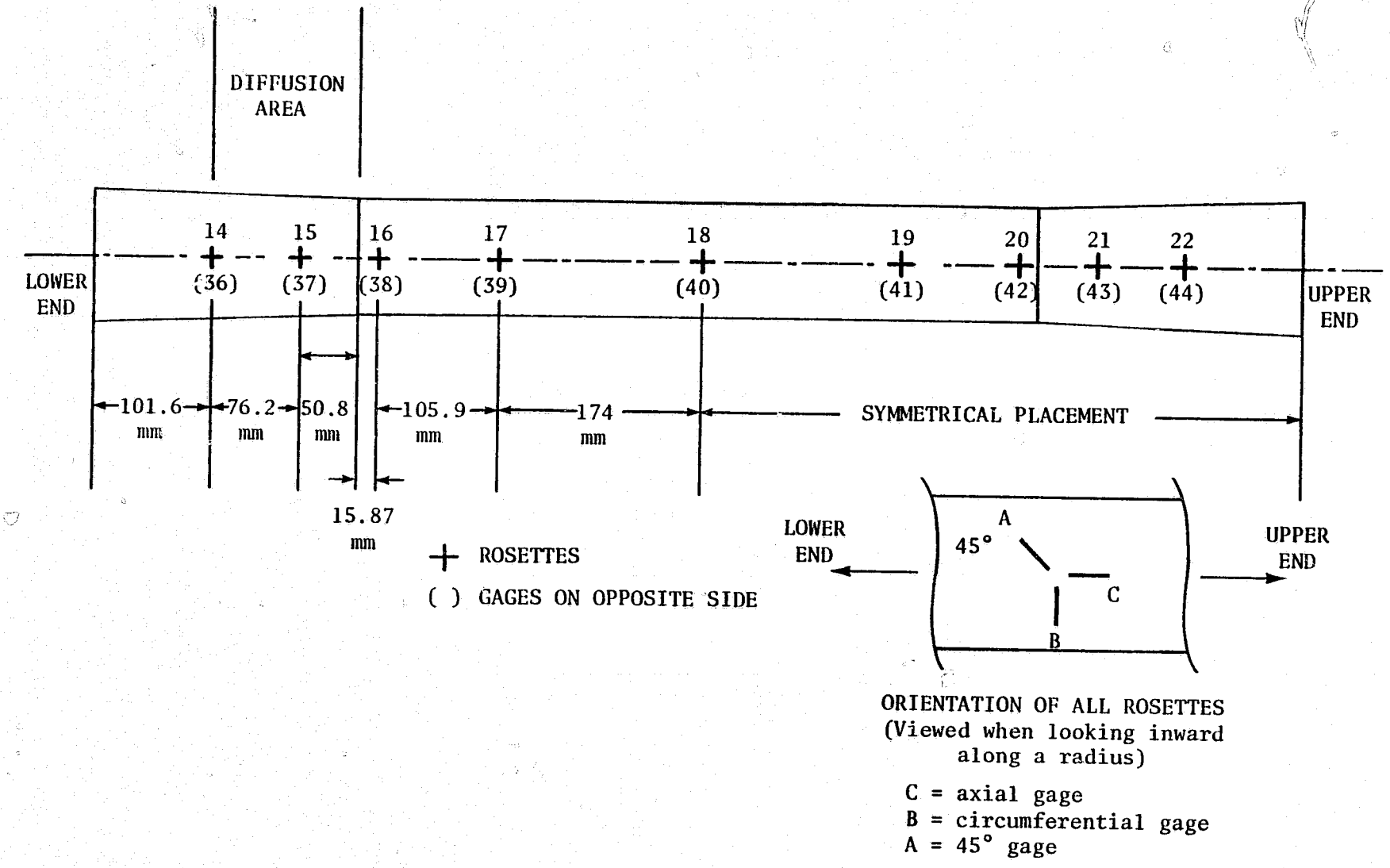

Figure 8. Side strain gage locations, right side view.

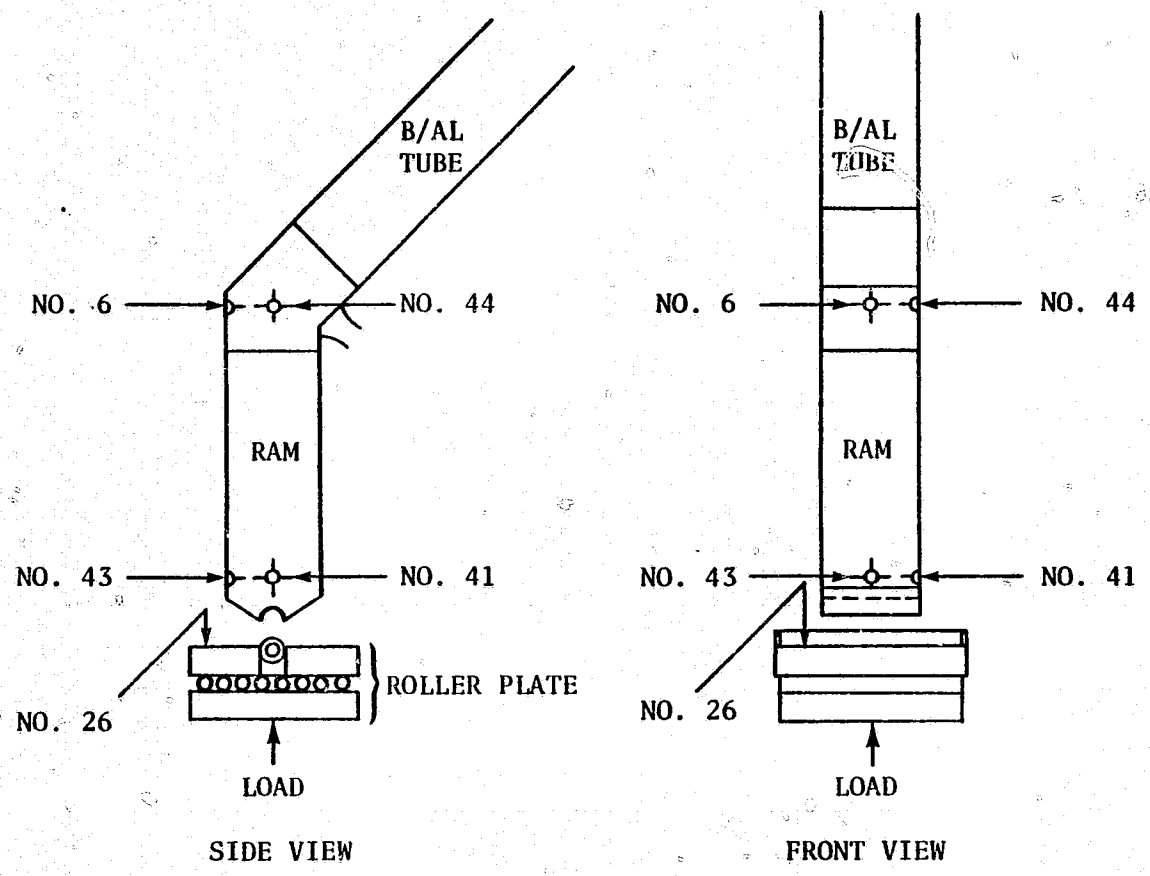

Figure 9. DCDT locations.

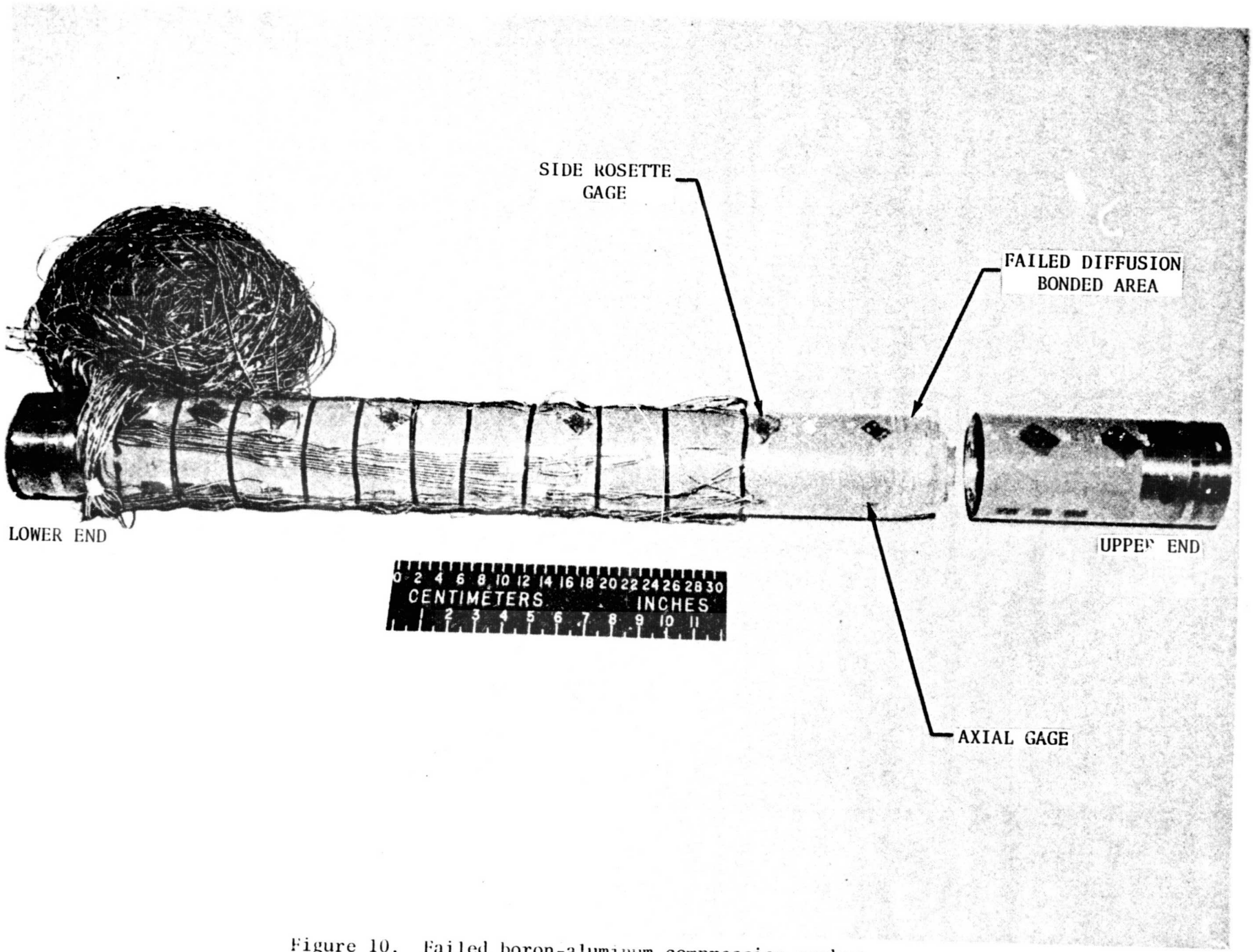

Figure 10. Failed boron-aluminum compression member.

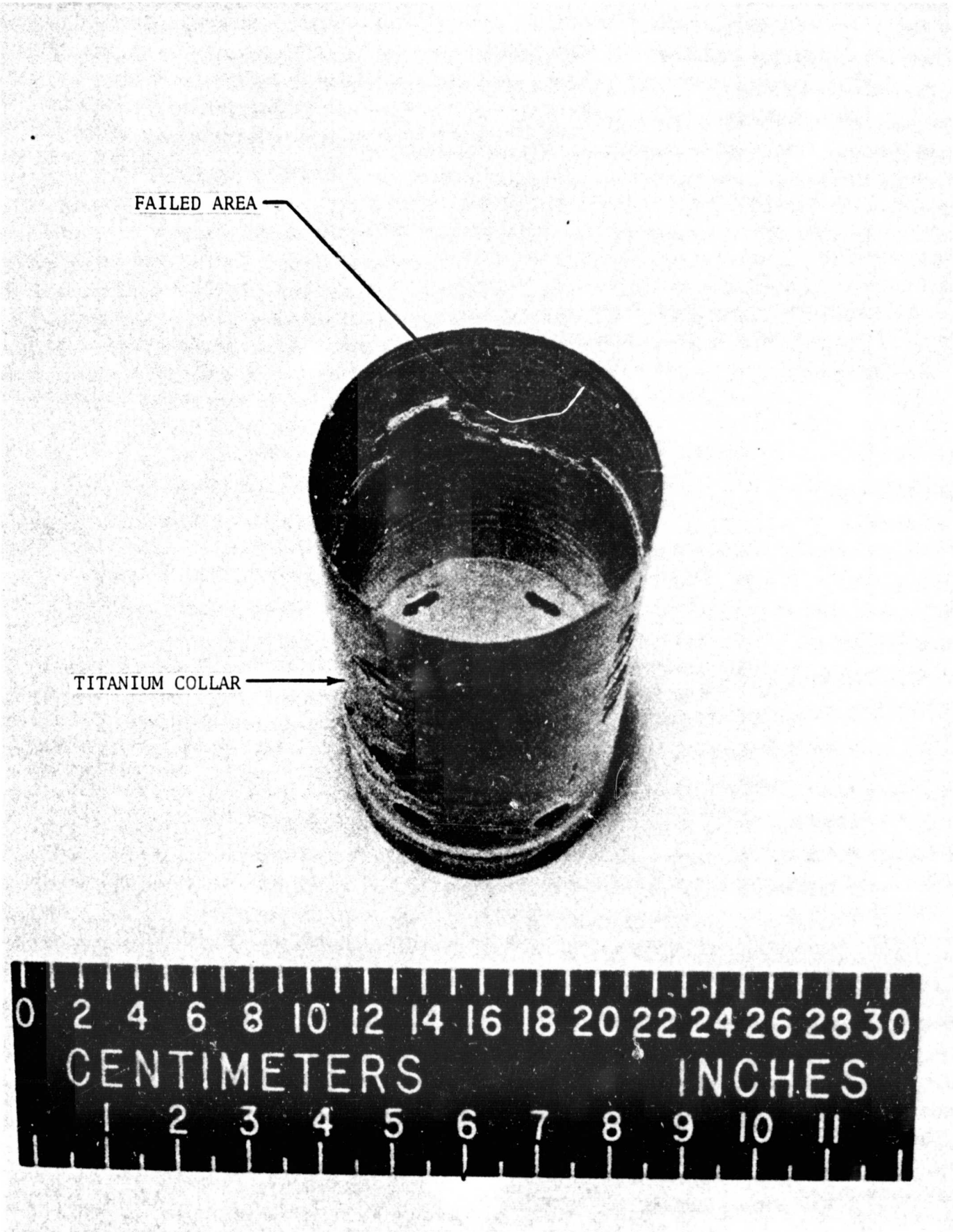

Figure 11. Detail of titanium end fitting after failure.

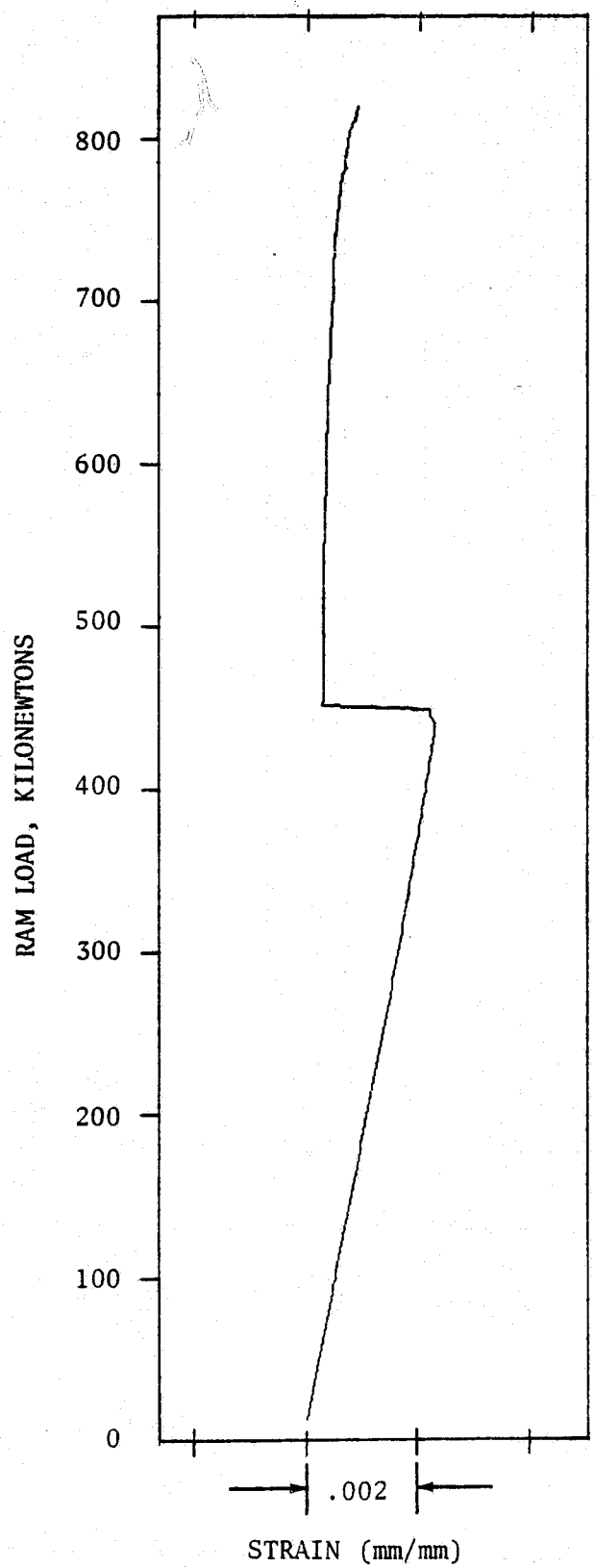

Figure 12. Load-strain behavior for strain gage No. 11.

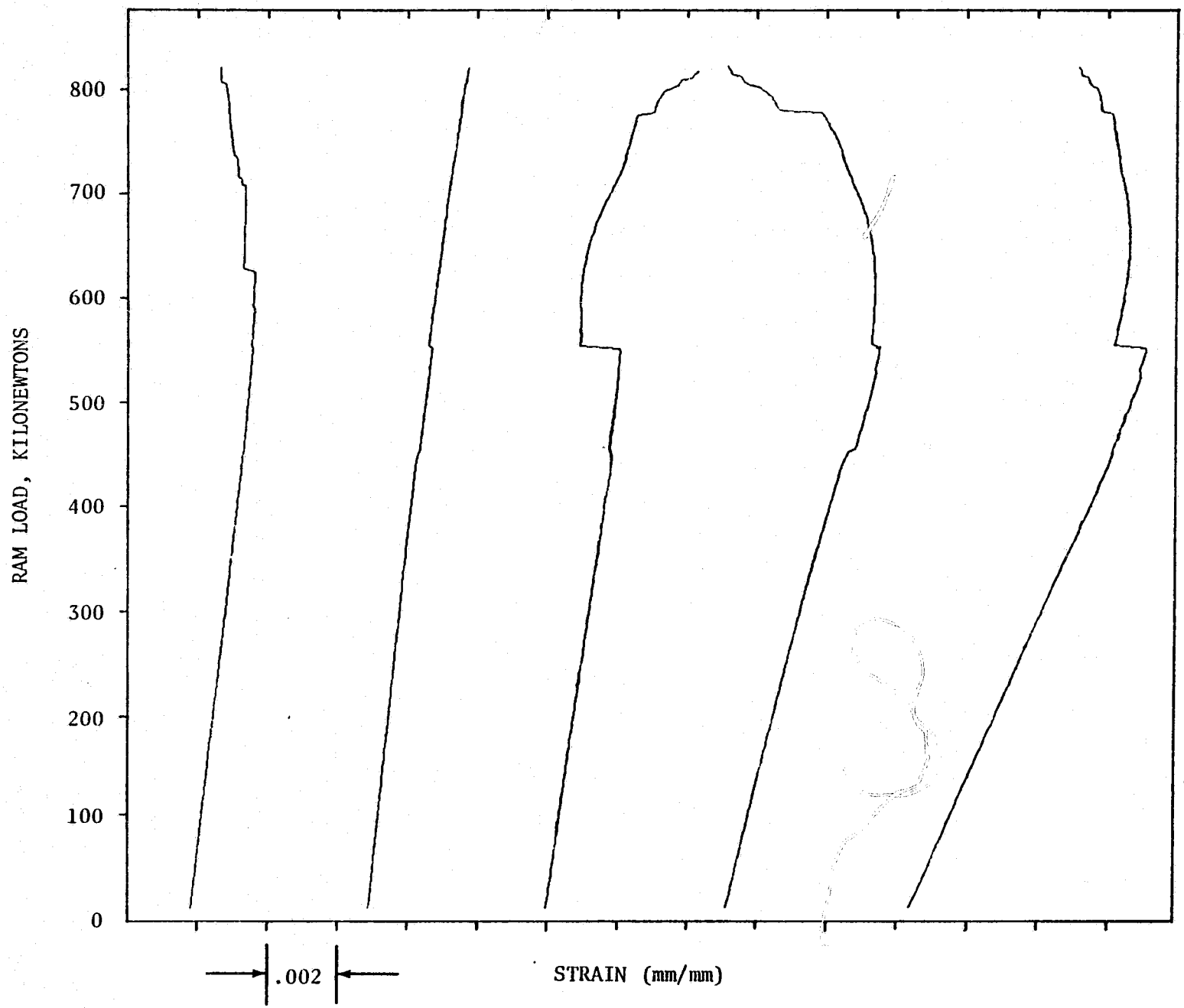

Figure 13. Load-strain behavior for strain gages 33, 42B, 43A, 43B, and 43C.

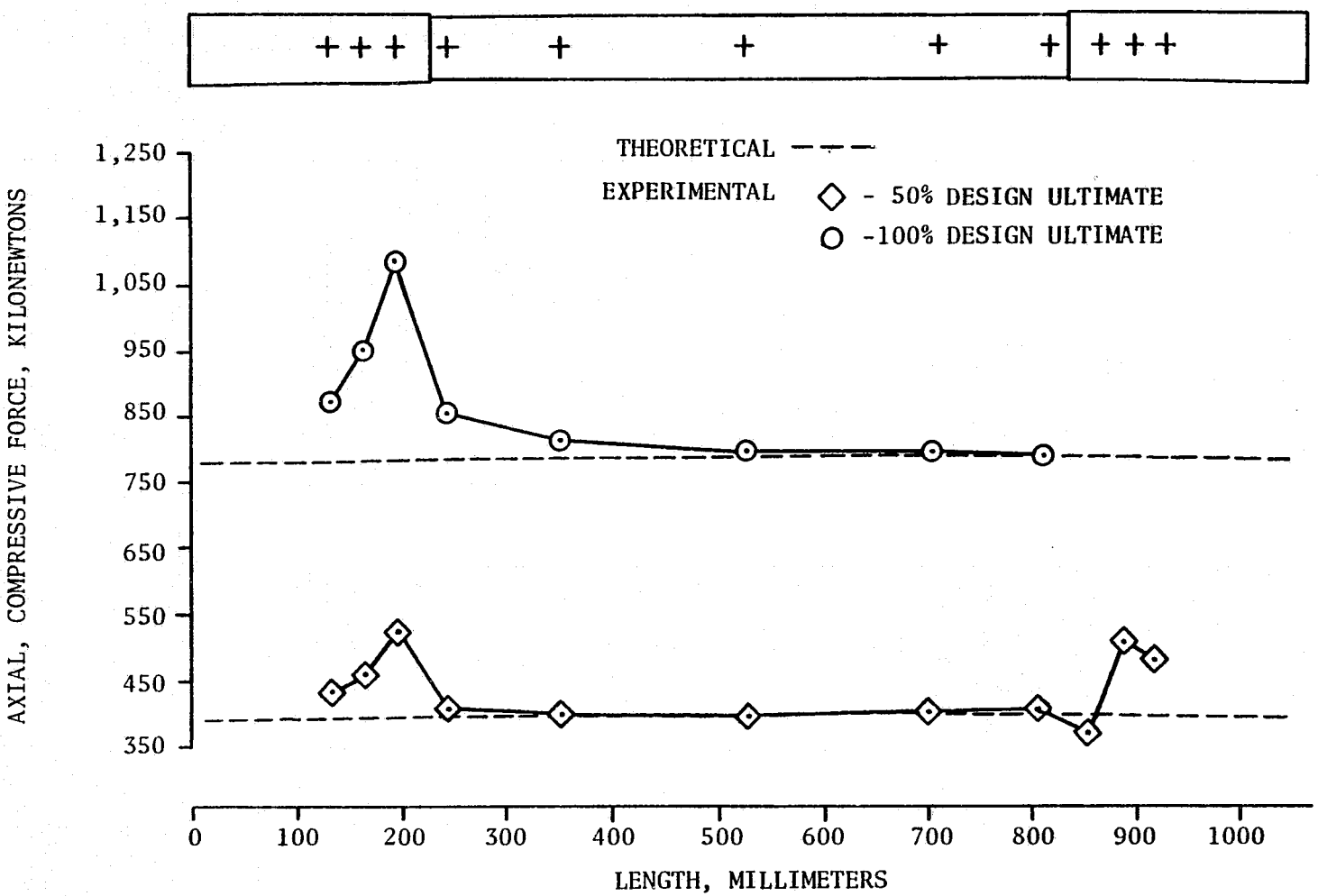

Figure 14. Axial force in compression tube using top and bottom gage pairs.

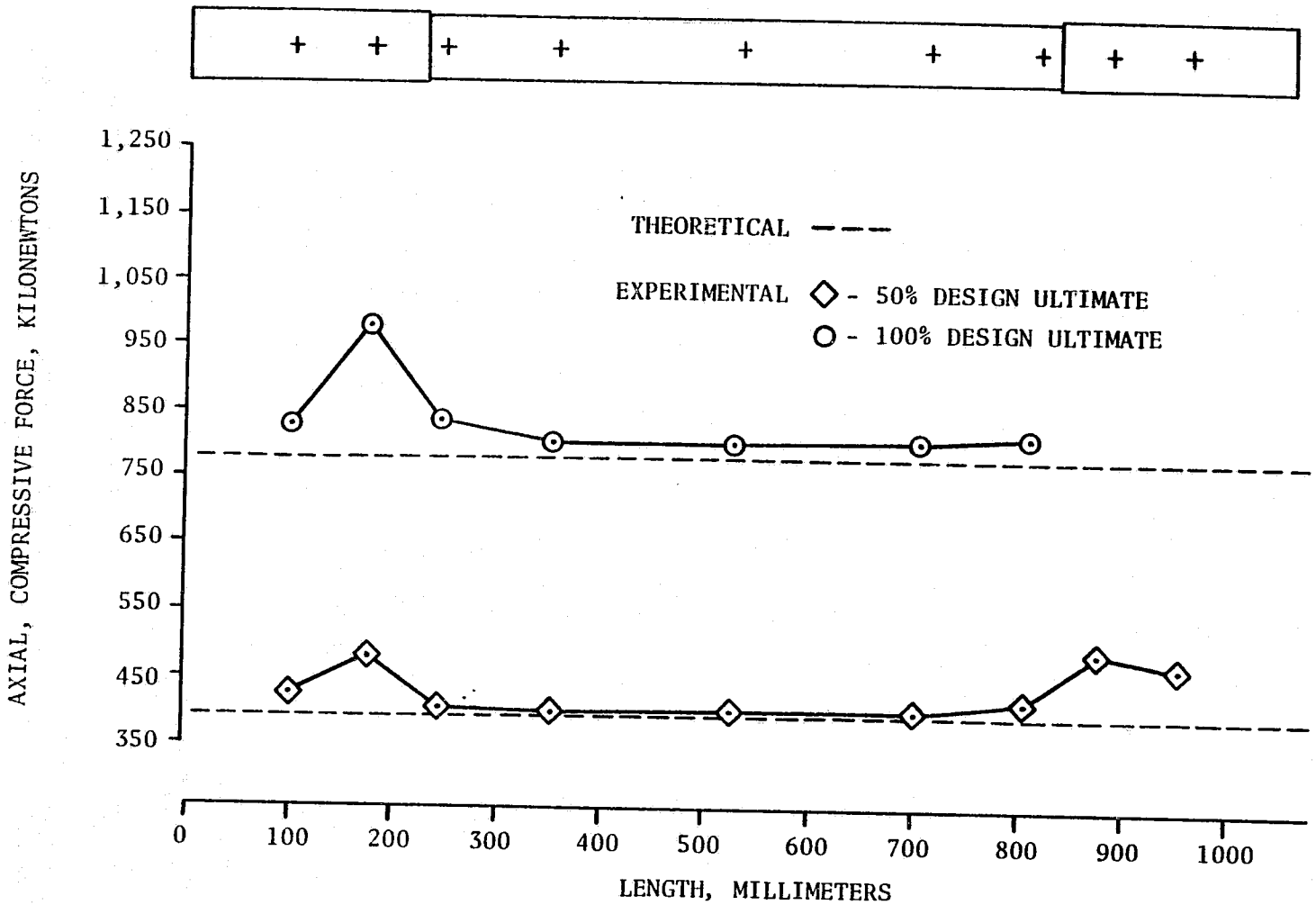

Figure 15. Axial force in compression tube using side-to-side gage pairs.

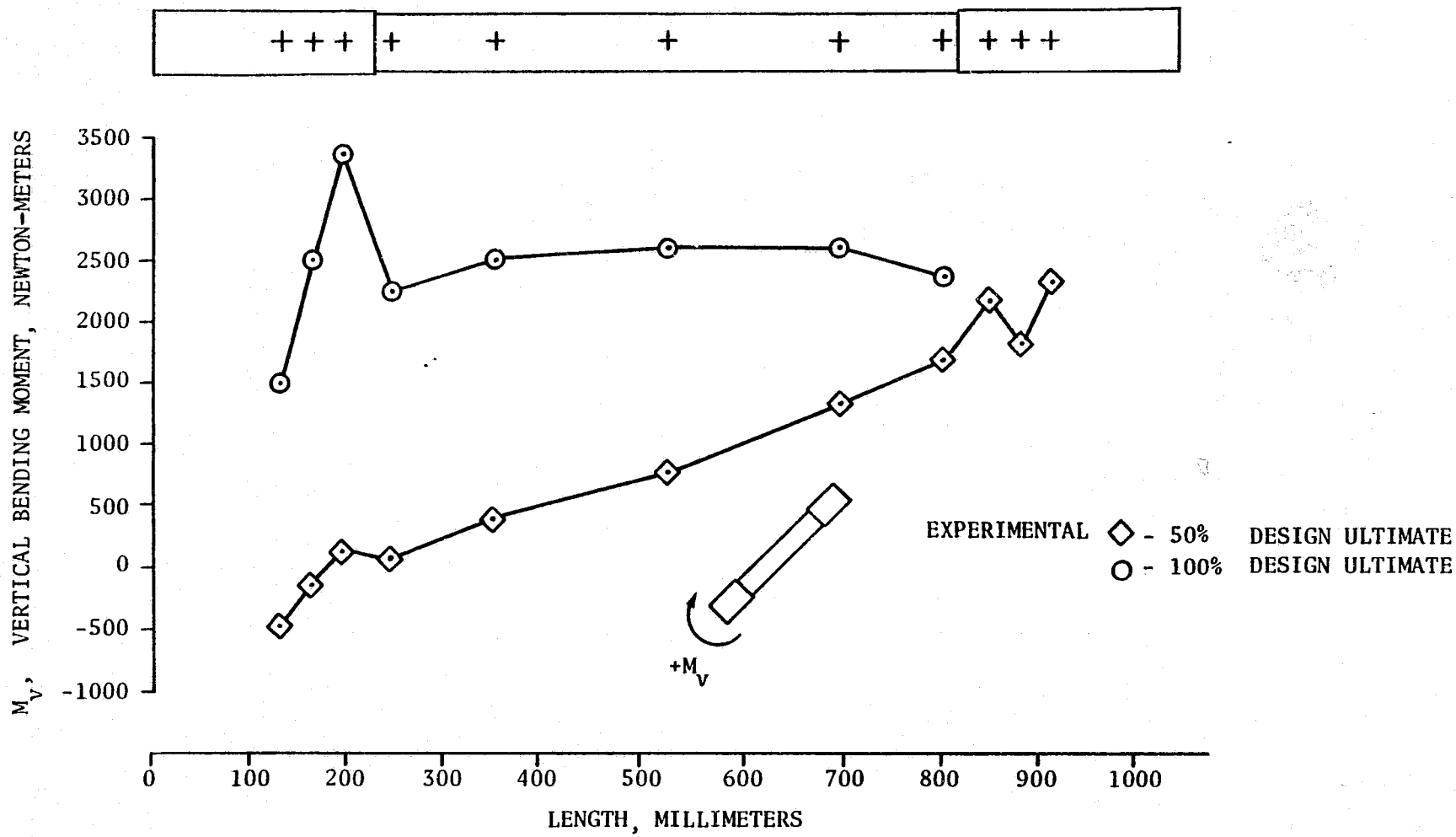

Figure 16. Vertical bending moment in compression tube.

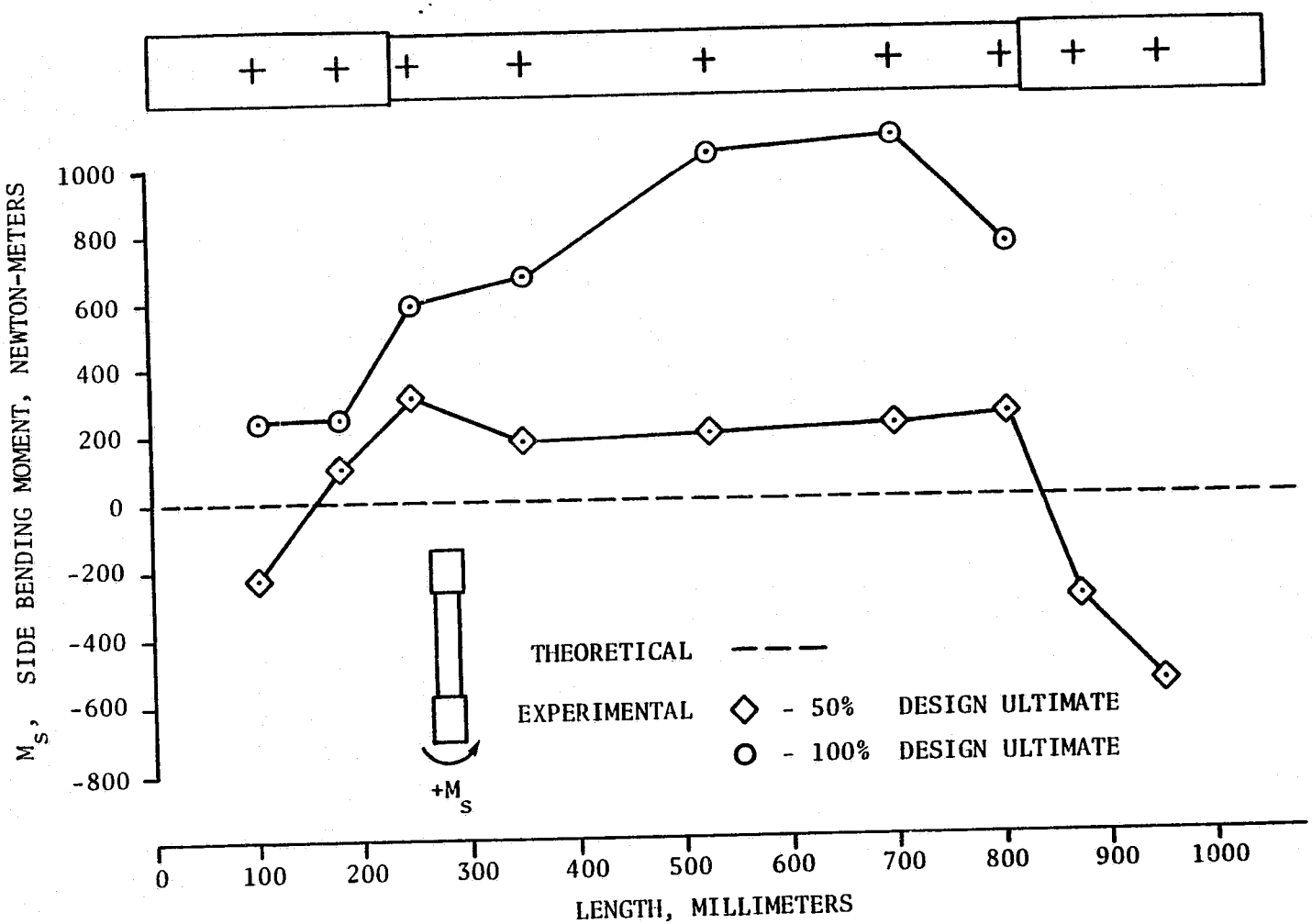

Figure 17. Side bending moment in compression tube.

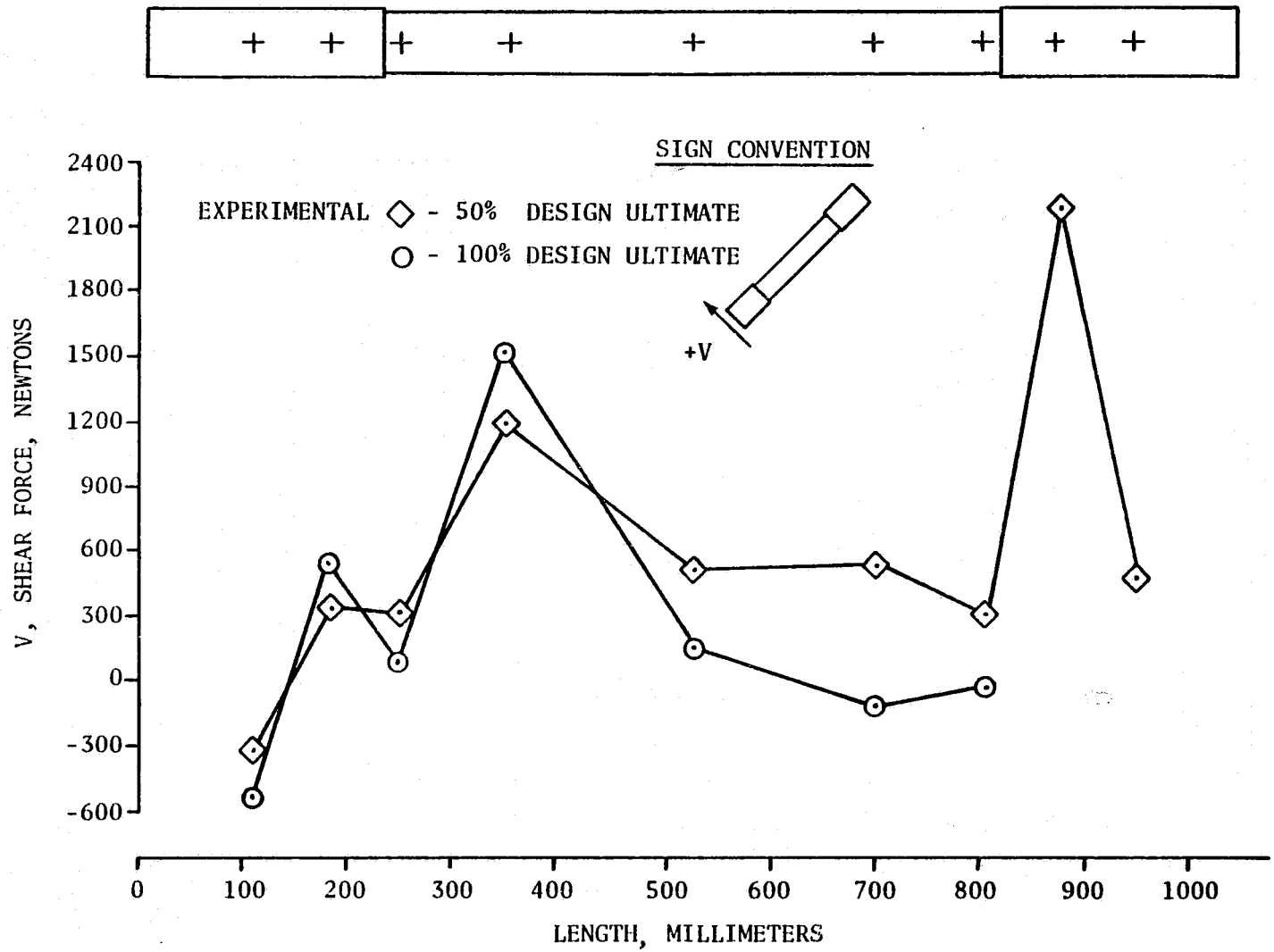

Figure 18. Shear force in compression tube.

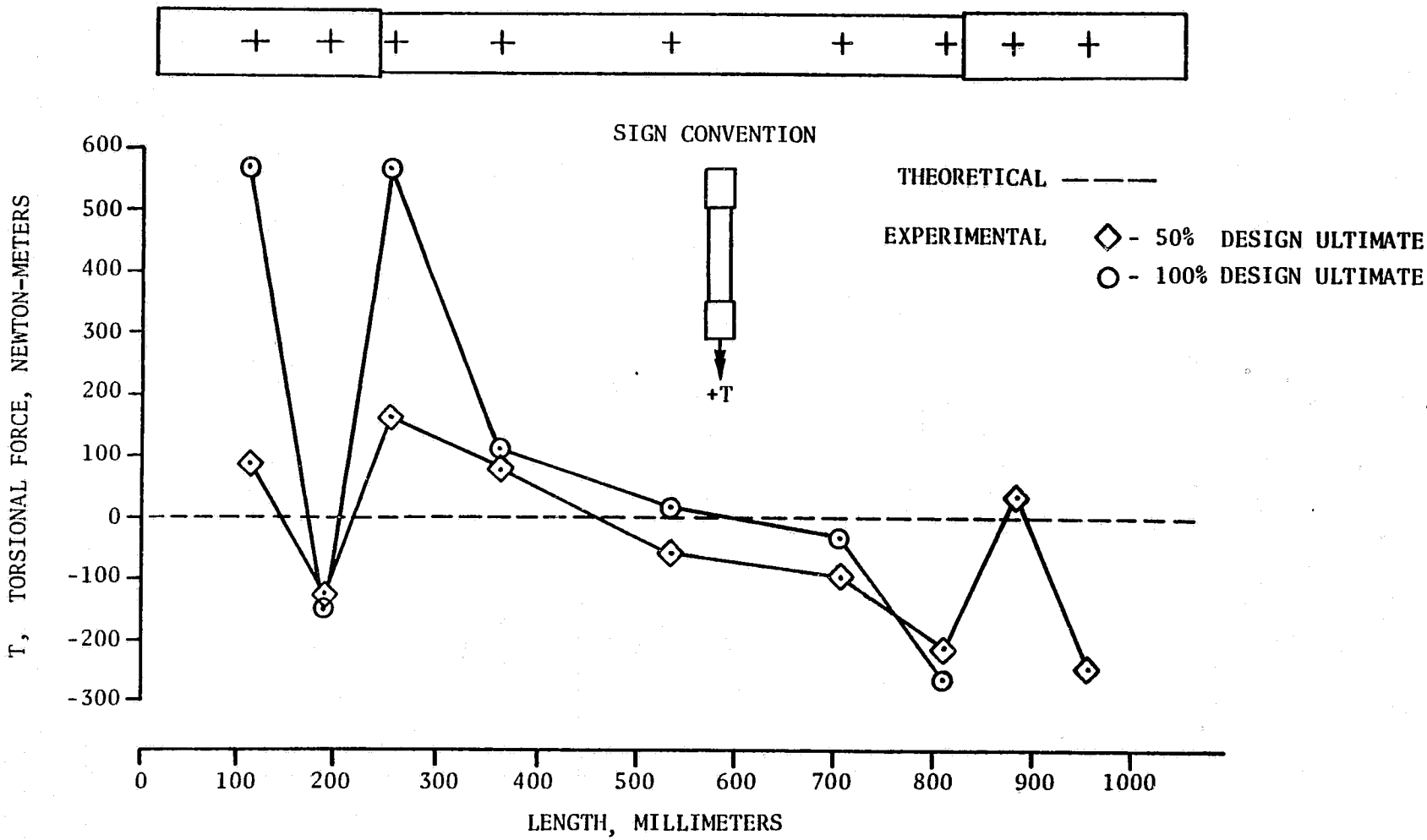

Figure 19. Torsion in compression tube.

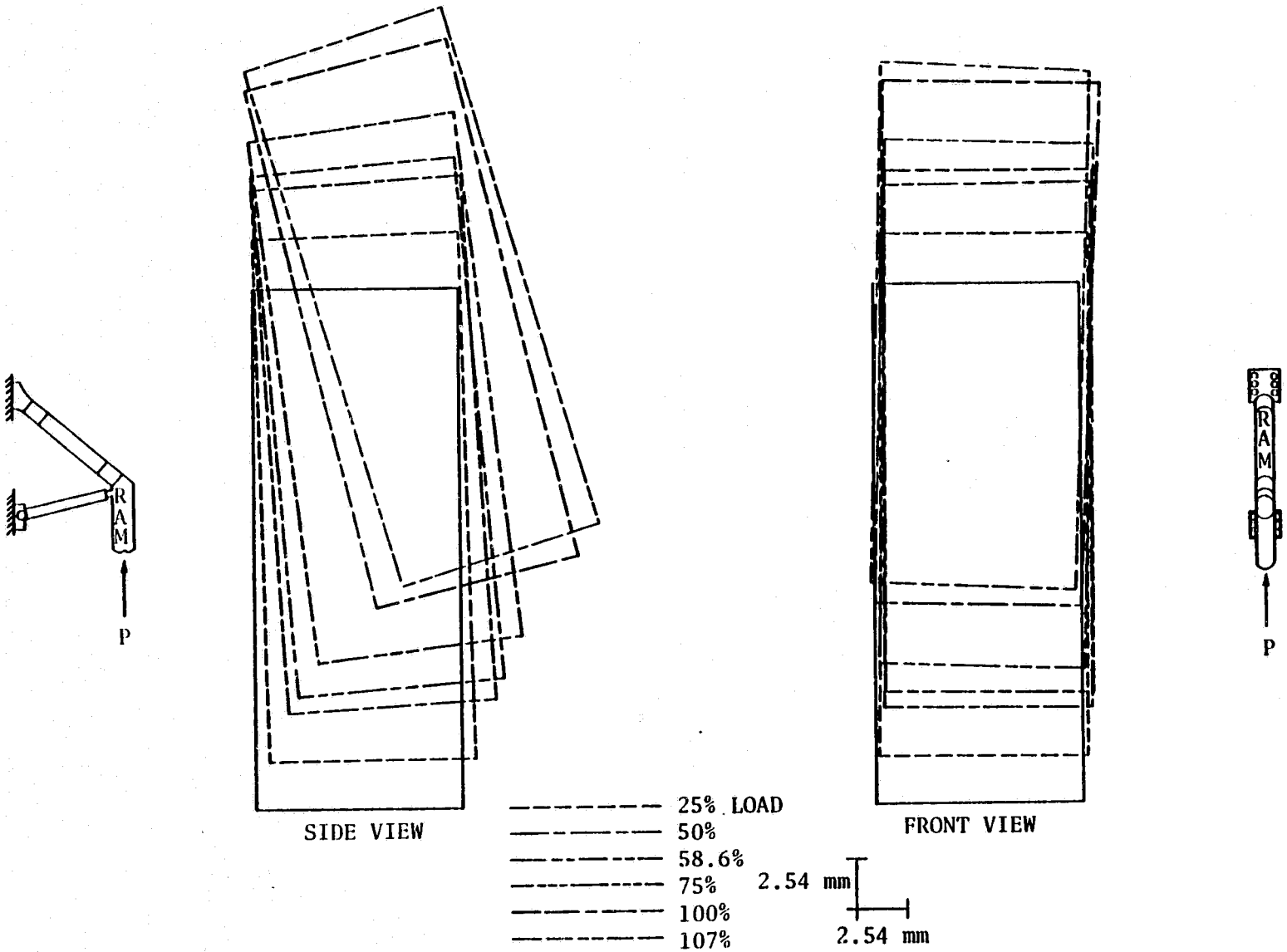

Figure 20. Displacement of ram and joint cluster assembly.

APPENDIX

The internal loads were initially computed using the value of E supplied by General Dynamics. This value of E gave axial load and vertical bending moment which were considerably less than predicted. As a check on E, a 101.6-mm-long segment was cut out of the compression tube. Four gages placed at 90° (uniaxially with fibers) around the circumference were used to measure compressive strains, and the section was loaded between two flat aluminum plates. In addition to having four strain measurements per compression test, the section was rotated 90° three times to average out any eccentricities in the loading mechanism or specimen. Load-strain characteristics were plotted on x-y recorders and the specimen was carefully measured to determine cross-sectional area. The load-strain curves were quite linear and the slopes of these curves, and the cross-sectional area, were used to compute E for each test. The values of E were averaged and the average value of E in the axial direction was determined to be 24.0×10^{10} N/m^2. The standard deviation among the values was $.5 \times 10^{10}$ N/m^2. The value of E taken from reference 2 was 19.29×10^{10} N/m^2.

To determine if this higher E was due to a higher than expected amount of boron, a volume fraction test was done with a shorter, 25.4-mm-long, segment. The volume percent was 52.2 percent boron. The volume percent in reference 2 was 47.1 percent boron. This higher percent of boron probably accounts for the higher value of E.

Careful examination of a small tube section revealed a thin ply region, which covered a very short distance of arc length, running the entire length of the tube. This seam was generated during fabrication of the tube. Figure A-1 shows an enlargement of both a normal cross-sectional segment of arc length and this thinner region. The thin region covered an arc length of 3.175 mm compared to the total circumferential distance of 355.6 mm and was not considered in the calculation of area used to determine E from the compression tests.

The elastic properties in the diffusion bond region were determined by the rule of mixtures according to the following formulas:

$$E_{equivalent} = \frac{E_{titanium} A_{titanium} + E_{boron\text{-}aluminum} A_{boron\text{-}aluminum}}{A_{total}}$$

$$G_{equivalent} = \frac{G_{titanium} A_{titanium} + G_{boron\text{-}aluminum} A_{boron\text{-}aluminum}}{A_{total}}$$

Table A-1 shows the equivalent values of E and G at various locations in the diffusion bond region. The areas and elastic constant used in the computations are taken from figure 1 of reference 2 since they could not be measured directly. Because the axial load is constant along the length of the tube, the value of E required to give the correct axial load is also shown in the table.

Table A-1. Rule-of-mixtures computations.

Location (mm)	Area (mm^2) Titanium	Area (mm^2) Boron-Aluminum	$E_{equivalent}$ (GN/m^2)	$E_{required}$ 50% (GN/m^2)	$E_{required}$ 100% (GN/m^2)	$G_{equivalent}$ (GN/m^2)
133.4	41.10	15.31	142.5	128.9	127.4	40.0
165.1	28.36	16.17	165.5	141.0	136.0	40.2
177.8	23.18	25.88	184.1	150.1	146.2	47.8
196.8	16.77	33.74	202.4	151.8	145.7	512.2
851.9	16.77	33.74	202.4	218.6	*	512.2
871.0	23.18	25.88	184.1	138.8	*	47.8
883.7	28.36	16.17	165.5	128.3	*	40.2
915.4	41.10	15.31	142.5	114.0	*	40.0

* Local failure in upper diffusion areas did not allow evaluation of loads at 100 percent ultimate design load.

Thinned Region

Normal Section

Figure A-1. Enlargement of compression tube wall sections.

REFERENCES

1. Corvelli, Nicholas; and Carri, Robert: Evaluation of Boron-Epoxy-Reinforced Titanium Tubular Truss for Application to a Space Shuttle Booster Thrust Structure. NASA TN D-6778, June 1972.

2. Robertson, A. R.: Design and Fabrication of a Boron/Aluminum Truss Member. Final rep., NASA1-13364, November 1974.